

## Article

# Controllable Construction of Amino-Functionalized Dynamic Covalent Porous Polymers for High-Efficiency CO<sub>2</sub> Capture from Flue Gas

Mingyue Qiu <sup>1</sup>, Haonan Wu <sup>1</sup>, Yi Huang <sup>1</sup>, Huijuan Guo <sup>1</sup>, Dan Gao <sup>2</sup>, Feng Pei <sup>3</sup>, Lijuan Shi <sup>1,\*</sup> and Qun Yi <sup>1,4,\*</sup> <sup>1</sup> School of Chemical Engineering and Pharmacy, Wuhan Institute of Technology, Wuhan 430205, China<sup>2</sup> School of Energy, Power and Mechanical Engineering, North China Electric Power University, Beijing 102206, China<sup>3</sup> Hubei Yihua Chemical Technology R&D Co., Ltd., Yichang 443208, China<sup>4</sup> Shanxi-Zheda Institute of Advanced Materials and Chemical Engineering, Taiyuan 030024, China

\* Correspondence: shilijuanwit@sina.com (L.S.); yq20071001@163.com (Q.Y.)

**Abstract:** The design of high-efficiency CO<sub>2</sub> adsorbents with low cost, high capacity, and easy desorption is of high significance for reducing carbon emissions, which yet remains a great challenge. This work proposes a facile construction strategy of amino-functional dynamic covalent materials for effective CO<sub>2</sub> capture from flue gas. Upon the dynamic imine assembly of N-site rich motif and aldehyde-based spacers, nanospheres and hollow nanotubes with spongy pores were constructed spontaneously at room temperature. A commercial amino-functional molecule tetraethylenepentamine could be facilely introduced into the dynamic covalent materials by virtue of the dynamic nature of imine assembly, thus inducing a high CO<sub>2</sub> capacity (1.27 mmol·g<sup>-1</sup>) from simulated flue gas at 75 °C. This dynamic imine assembly strategy endowed the dynamic covalent materials with facile preparation, low cost, excellent CO<sub>2</sub> capacity, and outstanding cyclic stability, providing a mild and controllable approach for the development of competitive CO<sub>2</sub> adsorbents.

**Keywords:** CO<sub>2</sub> capture; dynamic covalent polymer; imine exchange; amino functionalization



**Citation:** Qiu, M.; Wu, H.; Huang, Y.; Guo, H.; Gao, D.; Pei, F.; Shi, L.; Yi, Q. Controllable Construction of Amino-Functionalized Dynamic Covalent Porous Polymers for High-Efficiency CO<sub>2</sub> Capture from Flue Gas. *Molecules* **2022**, *27*, 5853. <https://doi.org/10.3390/molecules27185853>

Academic Editors: Yan'an Gao and Fei Lu

Received: 11 August 2022

Accepted: 5 September 2022

Published: 9 September 2022

**Publisher's Note:** MDPI stays neutral with regard to jurisdictional claims in published maps and institutional affiliations.



**Copyright:** © 2022 by the authors. Licensee MDPI, Basel, Switzerland. This article is an open access article distributed under the terms and conditions of the Creative Commons Attribution (CC BY) license (<https://creativecommons.org/licenses/by/4.0/>).

## 1. Introduction

Excessive CO<sub>2</sub> emissions from the burning of fossil fuels have caused a series of ecological and environmental problems [1,2]. Post-combustion capture of CO<sub>2</sub> from flue gases has been considered as one of the potential strategies for reducing carbon emissions [3,4]. Various CO<sub>2</sub> capture techniques, mainly including liquid ammonia absorption [5], membrane separation [6], and adsorption [7], have been widely developed. In particular, CO<sub>2</sub> adsorption by solids has the advantages of high recycling rate, simple operation, low equipment corrosion, and low energy consumption; thus, it is of high promise for low-energy CO<sub>2</sub> capture [8–10]. It is, therefore, of great significance for developing high-efficiency adsorbents with low cost, high capacity, and easy desorption, which yet remains a great challenge.

Great efforts have been made toward developing diverse kinds of CO<sub>2</sub> adsorbents, e.g., inorganic porous materials, covalent organic materials, and supramolecular organic materials [11]. Inorganic materials (e.g., zeolite [12], activated carbon [13], mesoporous silica [14], and mesoporous fibers [15]), despite having the advantages of high mechanical stability and regular porosity, mainly suffer from difficult structural functionalization and intrinsic acidic sites unfavorable for CO<sub>2</sub> adsorption [16]. Organic porous materials (e.g., polymers) have much more superior structural tunability compared to inorganic materials [17,18], but still suffer from complex preparation processes and high cost [19,20]. Alternatively, supramolecular organic materials, such as metal organic framework materials (MOFs) [21], hydrogen-bonded organic framework materials (HOFs) [22], covalent organic framework materials (COFs) [23], and coordination polymers [24], are generally constructed through

dynamic covalent and/or noncovalent bonding interactions. The dynamic noncovalent nature endows supramolecular organic materials with remarkable features such as simple preparation process, adjustable structure, and easy functionalization. In particular, dynamic covalent bonding (DCC) combines the stability and dynamic reversibility of covalent bonding, thus allowing the resultant dynamic covalent functional materials assembled to possess facile preparation, high stability, and promising functionalization [25–28].

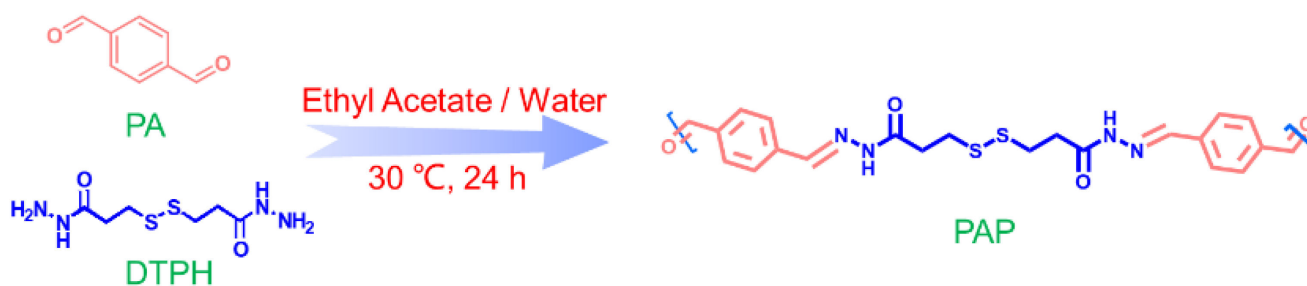
Amino functionalization of porous material has been considered as an efficient tool for improving CO<sub>2</sub> adsorption performance by taking advantage of the interaction between the amino group and CO<sub>2</sub> [29–33]. Traditionally, amino functionalization is mainly achieved through covalent grafting [34] and impregnation [35]. The former method often requires synthesis and activation of the as-prepared support (e.g., silica or zeolite) prior to grafting, complex chemical synthesis during the grafting process, and removal of solvent and/or unreacted reactants to activate pores [36]. The wet impregnation method tends to induce pore blockage and leaching of active component (e.g., organic amine or ionic liquid), and the liquid nature of active component increases both the viscosity of the composite material and the transfer resistance of CO<sub>2</sub>, thus generally inducing a relatively low CO<sub>2</sub> adsorption and/or low stability [37]. Moreover, the control over the content of functional sites and the nature of textural structures, which highly affects the CO<sub>2</sub> adsorption performance of the amine-functionalized materials, suffers from high challenges in both methods. Therefore, it is critical to explore a green and efficient approach for preparing amino-functionalized materials to promote CO<sub>2</sub> adsorption.

Herein, this work proposes a facile construction approach of functional dynamic covalent polymers through the dynamic imine assembly of N-site rich motif and aldehyde-based spacers for high-efficiency CO<sub>2</sub> capture. By virtue of the dynamic noncovalent nature, the structure of the dynamic covalent polymers can be readily regulated through the assembly process control, thus offering a feasible approach for promoting the CO<sub>2</sub> adsorption ability. Most importantly, amino-functional units can be readily introduced through the imine exchange method, thus offering a mild and controllable approach for the development of competitive CO<sub>2</sub> adsorbents.

## 2. Results and Discussion

### 2.1. Characterization of Dynamic Covalent Materials

A series of functional dynamic covalent nanomaterials were constructed via the self-assembly of 3,3'-dithiobis (propionyl hydrazine) (DTPH) and polyaldehyde at the ethyl acetate/water interface at 30 °C. Upon the self-assembly of DTPH and *p*-phthalaldehyde (PA), white powders were typically afforded (Scheme 1). To verify the successful imine assembly, the resultant samples were characterized by FT-IR technology. As shown in Figure 1, the N–H vibration peaks of DTPH at 3285 and 3326 cm<sup>-1</sup> disappeared in the dynamic covalent polymers [38], and a new peak assigned to C=N bond appeared at 1670 cm<sup>-1</sup> [39,40], indicating that DTPH was successfully assembled with PA.



**Scheme 1.** Schematic diagram of the synthesis of PAP at the ethyl acetate/water interface at 30 °C.

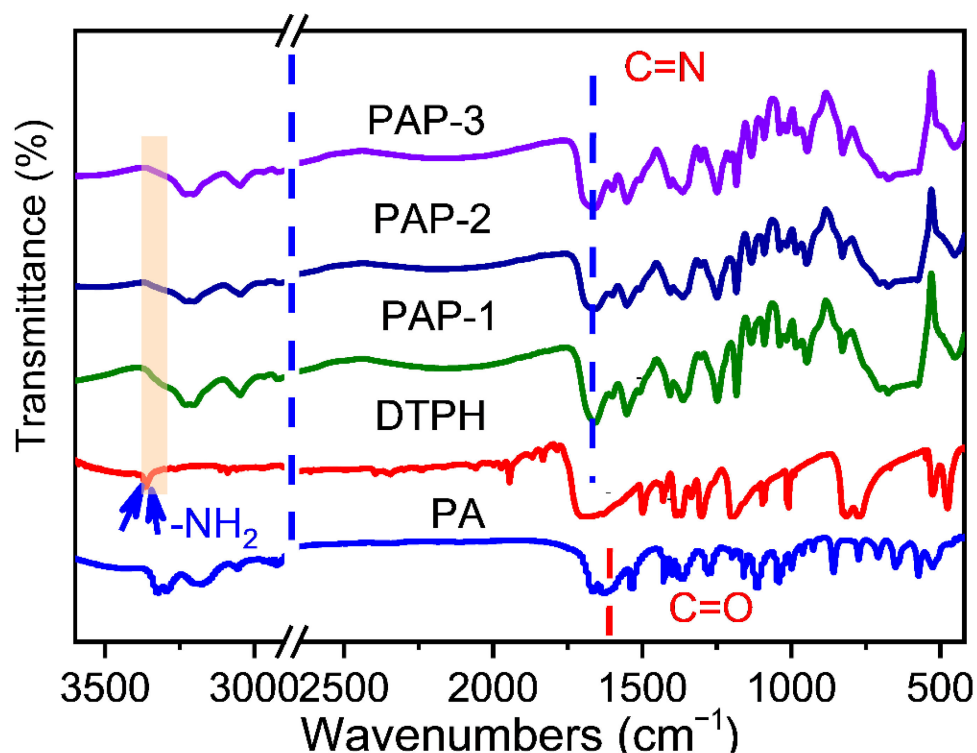


Figure 1. FT-IR spectra of PA, DTPH, and the resultant dynamic covalent materials PAP-X (X = 1, 2, 3).

Solid-state  $^{13}\text{C}$ -NMR characterization was used to further verify imine assembly. As shown in Figure 2, the characteristic signal at 163 ppm corresponded to the chemical shift of the C=N bond in PAP-1 [41,42]. In addition, the peak of the benzene ring derived from PA at 135 ppm and the peaks of C-C derived from DTPH at 35 ppm can be observed. The phenomena above proved the successful assembly of PA and DTPH through imine bonding.

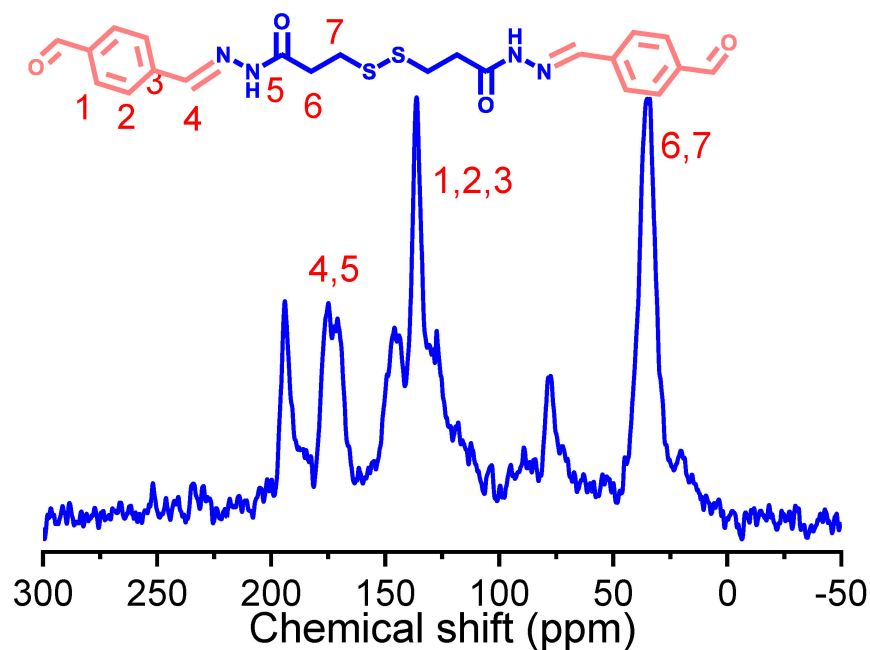
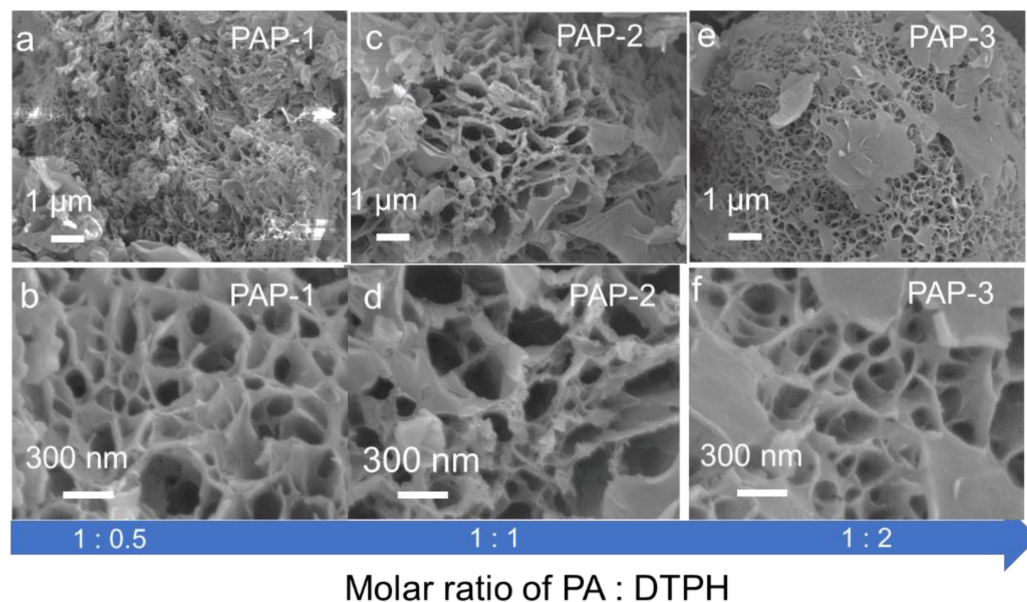


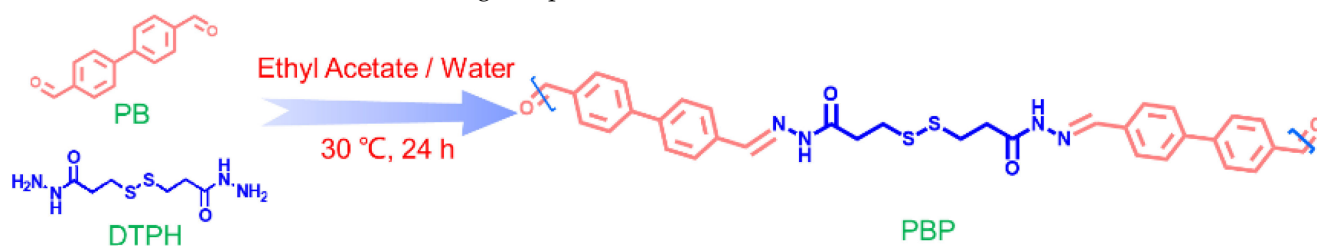
Figure 2. Solid-state  $^{13}\text{C}$ -NMR spectrum of PAP-1.

SEM observation revealed that nanoflowers with spongy pores were formed in the PAP samples with various molar ratios of PA and DTPH (Figure 3a,b), and the porous structures were considered of high promise for gas adsorption.



**Figure 3.** SEM images of (a,b) PAP-1, (c,d) PAP-2, and (e,f) PAP-3.

Similarly, the self-assembly of DTPH and 4,4'-biphenyldicarboxaldehyde (BPDA) could also be achieved (Scheme 2 and Figure 4). When the molar ratio of BPDA/DTPH was 1:0.5, porous nanospheres were formed (Figure 5a,b). With increasing content of DTPH, of great interest, nanospheres evolved into hollow nanotubes (Figure 5e,f). It can be noted that spongy porous structures were spread on the surface of the nanotubes, which was also beneficial for gas capture.



**Scheme 2.** Schematic diagram of the synthesis of PBP at the ethyl acetate/water interface at 30 °C.

The thermodynamic and kinetic analysis of supramolecular polymerization is of vital importance for understanding the pathway of structural regulation [43]. The effect of reaction time on the formation of the polymers was studied by taking PAP-3 as an example. It was found that powders could be formed within a quite short time. SEM characterization verified that a regular nanoflower morphology was formed within 0.5 h (see Figure 6). It can be seen that the dynamic imine assembly of PA and DTPH was under thermodynamic control rather than kinetic control [44,45].

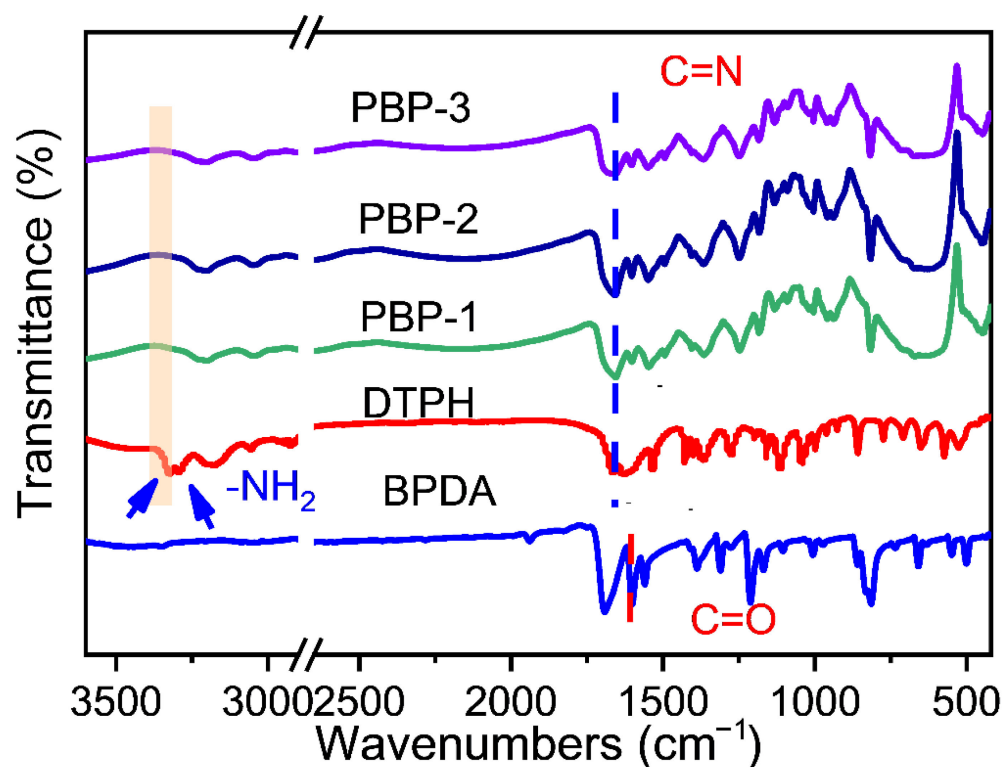


Figure 4. FT-IR spectra of BPDA, DTPH, and the resultant dynamic covalent materials PBP-X (X = 1, 2, 3).

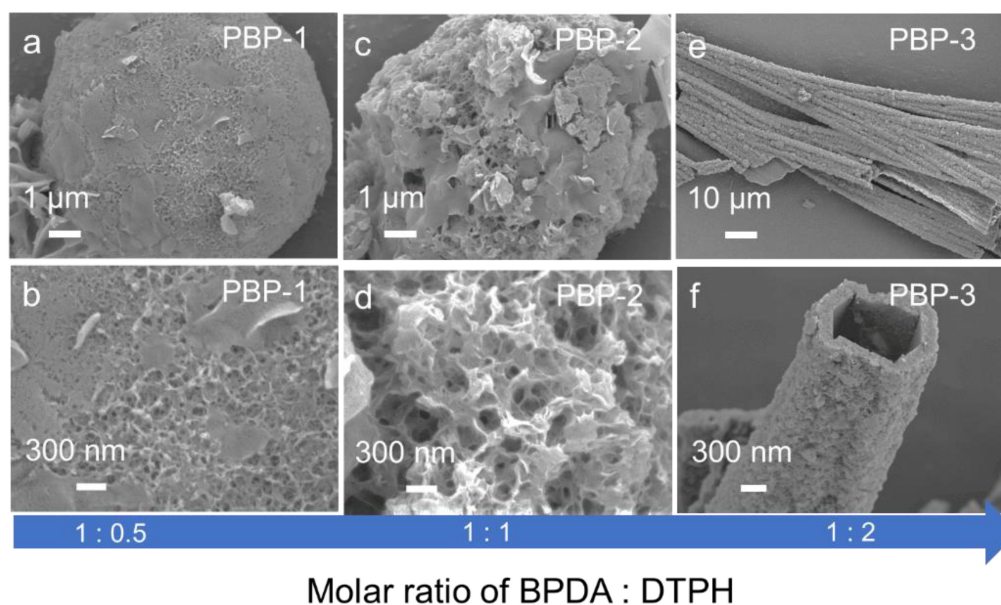


Figure 5. SEM images of (a,b) PBP-1, (c,d) PBP-2, and (e,f) PBP-3.

The crystal structures of the dynamic covalent polymers PAP and PBP were analyzed by X-ray diffraction (XRD). As can be seen from Figure 7, all the polymers had two broad diffraction peaks around  $17^\circ$  and  $25^\circ$ , indicating that the dynamic covalent polymer had an amorphous structure [46].

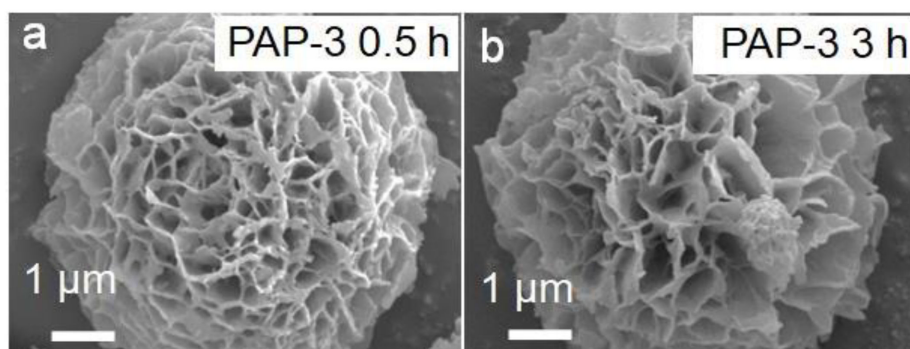


Figure 6. SEM images of dynamic covalent material PAP-3 formed at 0.5 h (a) and 3 h (b).

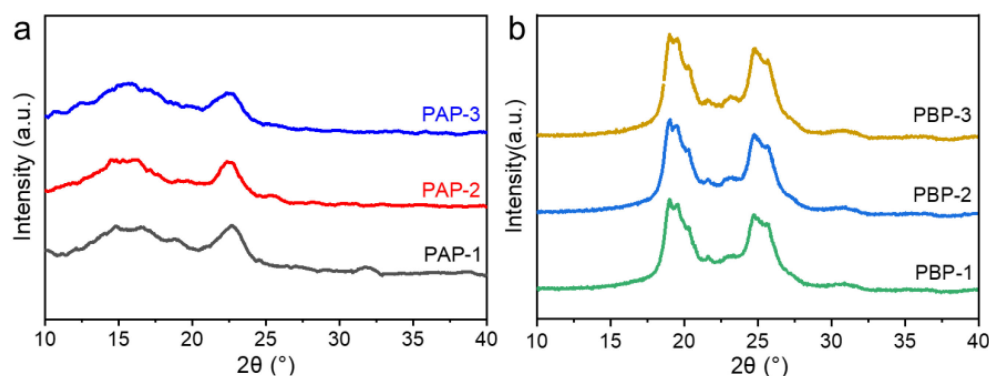


Figure 7. XRD spectra of (a) PAP and (b) PBP.

The maximum weight loss temperatures of PAP-1 and PBP-1 were both 292 °C, as shown in Figure 8, indicating the excellent thermal stability of the materials. The generation of imine from the reaction of amine and aldehyde is a reversible reaction that operates under thermodynamic control, through which the kinetically competing intermediate products are replaced by the thermodynamically most stable product after sufficient assembly time [47]. That is, imine assembly can afford a dynamic covalent material with excellent thermal stability under mild conditions.

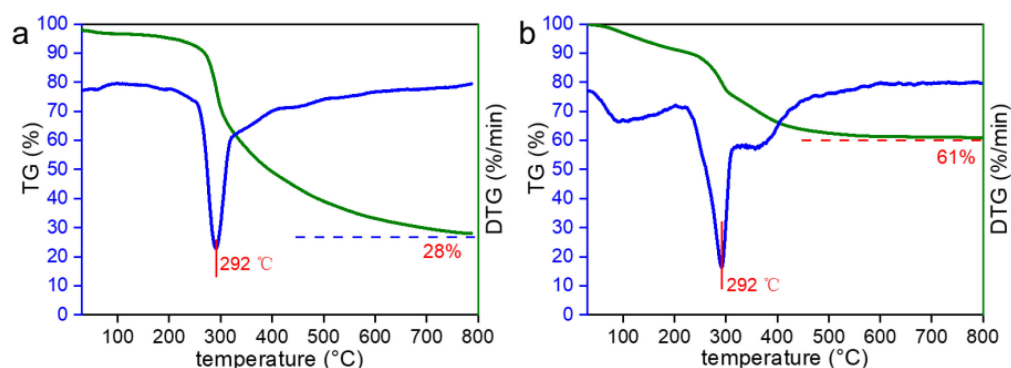


Figure 8. TGA and DTG curves of (a) PAP-1 and (b) PBP-1.

Porosity is a crucial factor for gas adsorption. The porous structures of PAP and PBP samples were characterized using N<sub>2</sub> adsorption-desorption. As shown in Figure 9a, the N<sub>2</sub> adsorption-desorption curves of the PAP samples presented a typical H4-type hysteresis loop, reflecting that the samples were composed of mesopores and/or macropores, which could be further confirmed by the analysis of pore volume (Table 1). This result is consistent with the SEM observation. H4-type N<sub>2</sub> adsorption-desorption curves with highly enlarged hysteresis loops could be observed for the PBP samples, especially for PBP-3. This phenomenon implies a relatively increased pore size in PBP-3, which was probably caused

by the formation of hollow structures. It can be seen that the specific surface area of PAP-2 was higher than that of PAP-1 and PAP-3. Compared to PAP-1 and PAP-3, the molar ratio of DTPH:PA in PAP-2 was 1:1, enabling DTPH and PA to react completely to form PAP, which was helpful for a high porosity. Moreover, there was no excess branch chain from DTPH and PA blocking the pore channels, which was also helpful for a higher specific surface area of PAP-2 than that of PAP-1 and PAP-3. For PBP-3, the relatively higher specific surface area was possibly contributed by the specific hollow nanotube structures covered with spongy pores, which had much higher pore volume than PBP-1 and PBP-2.

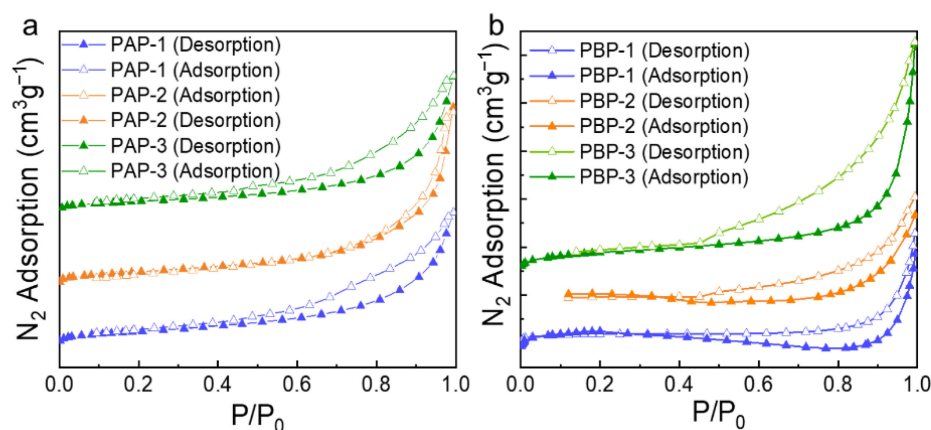


Figure 9.  $N_2$  adsorption and desorption curves of PAP (a) and PBP (b) samples.

Table 1. Specific surface area and pore volume of PAP and PBP samples.

Sample	$S_{BET}$ <sup>a</sup> ( $m^2 \cdot g^{-1}$ )	$V_{total}$ <sup>b</sup> ( $cm^3 \cdot g^{-1}$ )	$V_{meso}$ <sup>c</sup> ( $cm^3 \cdot g^{-1}$ )
PAP-1	72.57	0.27	0.27
PAP-2	77.91	0.36	0.36
PAP-3	58.20	0.28	0.28
PBP-1	17.27	0.09	0.19
PBP-2	33.12	0.16	0.16
PBP-3	63.12	0.32	0.32

<sup>a</sup> BET surface area. <sup>b</sup> Single-point pore volume calculated at relative pressure  $p/p_0$  of 0.99. <sup>c</sup>  $V_{total} - V_{micro}$ .

## 2.2. $CO_2$ Adsorption Performance

To mimic the post-combustion  $CO_2$  capture, the  $CO_2$  adsorption performances of the materials were detected from a simulated flue gas (a mixture of  $CO_2$  and  $N_2$  with 15 vol.%  $CO_2$ ) at 75 °C in a fixed-bed flow system equipped with a gas analyzer (see Figure 10a). On the whole, all samples presented a rapid adsorption within a short time and reached saturated adsorption within 300 s (Figure 10b). For PAP samples, the  $CO_2$  capacity was increased following the order of PBP-1 < PBP-2 < PAP-1 < PAP-3 < PAP-2 < PBP-3, which was overall positively correlated with their specific surface areas (see Table 1). Amongst these samples, PBP-3 presented the maximum  $CO_2$  capacity ( $0.84 \text{ mmol} \cdot g^{-1}$ ) although its surface area was somewhat lower than those of PAP-1 and PAP-2 (see Table 2). This result was probably due to the competitive effect of physisorption and chemisorption [48]. On one hand, the low specific surface area was not in favor of physisorption. On the other hand, however, chemisorption was gradually enhanced caused by the relatively high content of N-site rich motif DPTH, which could counteract the decrease in physisorption.

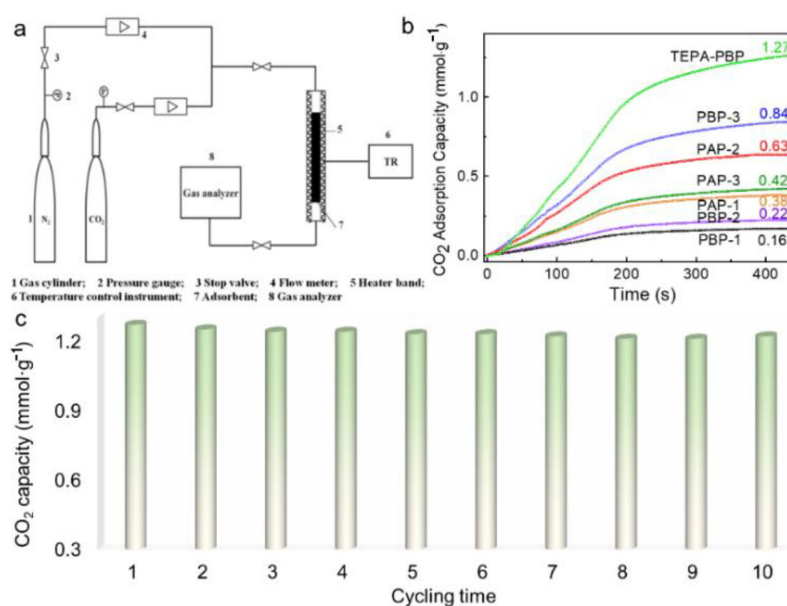


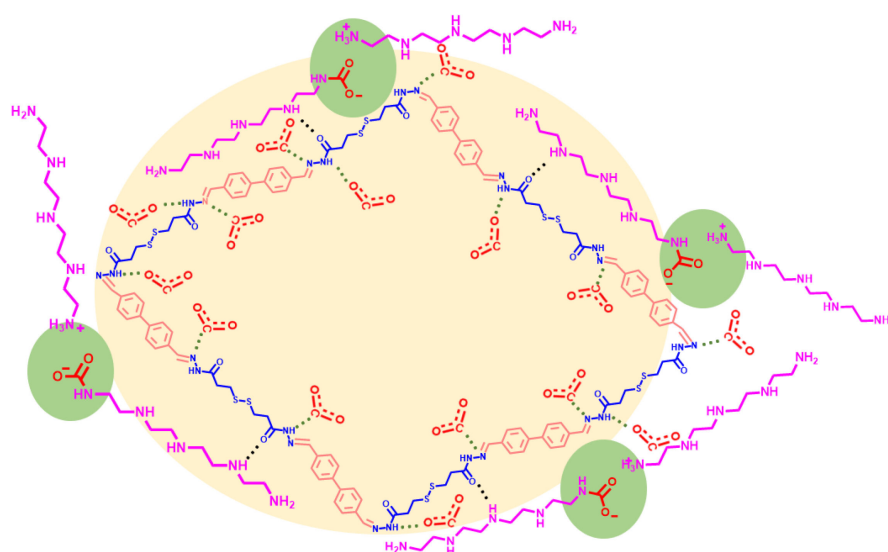
**Figure 10.** (a) Schematic diagram of the fixed-bed flow system. (b) CO<sub>2</sub> adsorption curves of PAP and PBP samples from a gas mixture of CO<sub>2</sub> (15 vol.%) / N<sub>2</sub> at 75 °C. (c) Ten cycles of CO<sub>2</sub> capacity of TEPA-PBP from a gas mixture of CO<sub>2</sub> (15 vol.%) / N<sub>2</sub> at 75 °C.

**Table 2.** CO<sub>2</sub> adsorption capacity of different adsorbents.

Entry	Adsorbent	CO <sub>2</sub> Capacity (mmol·g <sup>-1</sup> )	CO <sub>2</sub> Capacity (wt.%)
1	PAP-1	0.38	1.67
2	PAP-2	0.63	2.77
3	PAP-3	0.42	1.85
4	PBP-1	0.16	0.70
5	PBP-2	0.22	0.97
6	PBP-3	0.84	3.70
7	TEPA-PBP	1.27	5.59

To further improve the CO<sub>2</sub> performance of the dynamic covalent samples, amino-functional molecule tetraethylenepentamine (TEPA) was further introduced on PBP. It can be noted that the direct assembly of TEPA and DTPH failed to afford any solid powder. By virtue of the dynamic nature of imine assembly, TEPA can be facily grafted on PBP or even replace DPTH through imine exchange [49,50]. Benefiting from the many more active sites in TEPA than that in DPTH, as expected, the CO<sub>2</sub> capacity of the TEPA-modified PBP-3 sample (named TEPA-PBP) could reach up to 1.27 mmol·g<sup>-1</sup> (Figure 10b), 1.5 times that of bulk PBP-3. The high adsorption capacity for TEPA-PBP was mainly caused by the porous property and good affinity of amino/acylamide groups. The amino groups could act as chemisorbed sites to react with CO<sub>2</sub> to form ammonium carbamate [51], and acylamide and imine groups could adsorb CO<sub>2</sub> under the effect of hydrogen bonding and electrostatic attraction, respectively (see Scheme 3) [51].

The cyclic stability was also crucial for the industrial application of an adsorbent. The cyclic stability of TEPA-PBP was investigated by performing 10 cycles of CO<sub>2</sub> adsorption at 75 °C. It can be seen that the CO<sub>2</sub> adsorption capacity of TEPA-PBP remained constant in each cycle (Figure 10c), reaching 1.21 mmol·g<sup>-1</sup> of CO<sub>2</sub> uptake after 10 cycles, verifying the excellent adsorption reversibility of TEPA-PBP.



**Scheme 3.** Mechanistic diagram of CO<sub>2</sub> absorption on dynamic covalent material TEPA-PBP.

The CO<sub>2</sub> adsorption performance of the designed material TEPA-PBP was compared with typical reported adsorption materials. As shown in Table 3, TEPA-PBP exhibited competitive CO<sub>2</sub> adsorption capacity from flue gas. Superior to most reported adsorbents, moreover, the material developed in this work exhibits facile preparation, low cost, and a metal-free nature, thus promoting its availability in practical application.

**Table 3.** Comparison of the CO<sub>2</sub> adsorption performance of TEPA-PBP with advanced adsorbents.

Entry	Adsorbent	Adsorption Temperature (°C)	CO <sub>2</sub> Capacity (mmol·g <sup>-1</sup> )	Ref.
1	TEPA-PBP	75	1.27	This work
2	OC700	25	1.36	[52]
3	0.44PEI@AOMC	75	1.14	[53]
4	PEI-MgO	30	0.54	[54]
5	SA-PEI-TEA	70	0.61	[55]
6	PE/PP-g-PVBC-EDA	50	2.7	[56]

### 3. Materials and Methods

#### 3.1. Materials

Dimethyl 3,3'-dithiobispropionate (98%) and tetraethylenepentamine (98%) were purchased from Shanghai Titan Technology Co., Ltd., Shanghai, China. *p*-Phthalaldehyde (PA, 98%) and 4,4'-biphenyldicarboxaldehyde (BPDA, 98%) were purchased from Innochem Chemical Co., Beijing, China. CO<sub>2</sub> (99.99%) and N<sub>2</sub> (99.99%) were purchased from Taiyuan Steel Co., Shanxi, China.

#### 3.2. Synthesis of Materials

##### 3.2.1. Synthesis of 3,3'-Dithiobis(propionyl Hydrazine)

Dimethyl 3,3'-dithiodipropionate (12.01 g, 50.4 mmol) was added to anhydrous methanol (90 mL), followed by the addition of hydrazine hydrate (20.59 g, 403.2 mmol). After stirring at room temperature for 24 h, a white solid (3,3'-dithiobis(propionyl hydrazine), DTPH) was obtained by centrifugation, washed with methanol (30 mL × 2) and diethyl ether (30 mL × 2), and then dried in vacuum at 50 °C for 12 h. <sup>1</sup>H-NMR (δ<sub>ppm</sub>, 400 MHz, DMSO-d<sub>6</sub>): 9.09 (s, 1H), 4.20 (m, 2H), 2.88 (m, 2H), 2.40 (m, 2H).

### 3.2.2. Synthesis of PAP-X

PA (0.78 g, 3.3 mmol) was dissolved in 15 mL of ethyl acetate at 30 °C, and the solution was slowly added to 15 mL of DTP aqueous solution (0.45 g, 3.3 mmol). The two-phase system was sealed and left standing at 30 °C for 24 h. White powder was collected by centrifugation, washed with water (30 mL × 3) and ethyl acetate (30 mL × 3), and then dried in vacuum at 70 °C for 12 h. The samples with different molar ratios of PA/DTP (i.e., 1:0.5, 1:1, and 1:2) were prepared and named PAP-1, PAP-2, and PAP-3, respectively.

### 3.2.3. Synthesis of PBP-X

PBP-1 was synthesized following a similar procedure with PAP-1 under the reaction of BPDA and DTP at a molar ratio of 1:0.5. The samples with different molar ratios of BPDA/DTP (i.e., 1:0.5, 1:1, and 1:2) were prepared and named PBP-1, PBP-2, and PBP-3, respectively.

### 3.2.4. Synthesis of TEPA-PBP

Tetraethylenepentamine (TEPA, 0.03 g, 158 mmol) was dissolved in 15 mL of methanol and stirred at room temperature for 2 h. Then, 0.50 g of PBP-3 was added to the above solution under stirring at room temperature for 8 h. The precipitate was collected by centrifugation, washed with methanol (5 mL × 2) and water (5 mL × 2) in turn, and dried at 60 °C for 12 h.

## 3.3. Characterizations

The microscopic structures of samples were observed by scanning electron microscopy (SEM) on a ZEISS MERLIN CoMPact (Zeiss, Jena, Germany). Fourier-transform infrared (FT-IR) spectra were recorded on a Tensor 27 spectrometer (Bruker, Billerica, MA, USA) over a KBr pellet in the region of 4000–400 cm<sup>-1</sup>. X-ray diffraction (XRD) patterns were acquired in the range of 2θ = 10°–80° with scanning rate of 5°/min on PANalytical Empyrean (Almelo, The Netherlands). Thermogravimetry analysis (TGA) was conducted using an STA 449 F3 Jupiter<sup>®</sup> instrument (Netzsch, Selb, Germany) at a heating rate of 10 °C/min in N<sub>2</sub> atmosphere. The specific surface areas and pore structures of samples were measured on a Brunauer-Emmett-Teller (BET) apparatus (JW-BK200, Beijing, China). The micropore size distribution was calculated using the t-plot method, the mesopore size distribution was calculated using the BJH method, and the specific surface area was analyzed using the BET equation.

## 3.4. CO<sub>2</sub> Adsorption Capacity Evaluation

The CO<sub>2</sub> adsorption performances were determined in a fixed-bed flow system equipped with a gas analyzer (Gasboard-3100, Wuhan Cubic Optoelectronics Co., Ltd., Wuhan, China.). Typically, 0.5 g samples were placed in a column with diameter of 0.8 cm and heated to 100 °C in N<sub>2</sub> (99.999%) at a flow rate of 100 mL·min<sup>-1</sup> for 1 h. Then, the column was cooled to 75 °C, and a gas mixture of CO<sub>2</sub> (15 vol.%) and N<sub>2</sub> flowed through the column. The total pressure was 1 bar, and the CO<sub>2</sub> pressure was 0.15 bar. The CO<sub>2</sub> concentration was recorded every 1.0 s until returning to 15 vol.%. After adsorption, the column was heated to 120 °C for 1 h in N<sub>2</sub> (99.999%) at a flow rate of 100 mL·min<sup>-1</sup> to achieve CO<sub>2</sub> desorption. The CO<sub>2</sub> adsorption capacity ( $q_m$ , mmol·g<sup>-1</sup>) of the samples at a certain time ( $t$ , s) was calculated using Equation (1) [57].

$$q_m = \frac{Q}{M_{ad}} \int_0^t (C_0 - C_t) dt \times \frac{T_0}{T} \times \frac{1}{V_m} \quad (1)$$

where  $Q$  is the flow of the mixture (mL·min<sup>-1</sup>),  $M_{ad}$  is the mass of adsorbents,  $t$  is the adsorption time (s),  $C_0$  and  $C_t$  are the CO<sub>2</sub> concentrations at the inlet and outlet,  $T$  is the adsorption temperature (K), and  $V_m$  is the standard molar volume (22.4 L·mol<sup>-1</sup>,  $T_0 = 0$  °C).

#### 4. Conclusions

Through dynamic covalent assembly, *N*-site rich polymers were successfully constructed via the self-assembly of 3,3'-dithiobis (propionyl hydrazine) and polyaldehyde at the ethyl acetate/water interface at 30 °C. By regulating the type and ratio of polyaldehyde, nanospheres and hollow nanotubes with spongy pores were controllably formed. The dynamic covalent materials presented good thermal stability with a maximum decomposition temperature of ca. 292 °C. Tetraethylenepentamine with rich amino-functional groups was successfully grafted onto PBP at room temperature and provided rich chemisorption sites, such that the functional dynamic covalent polymer had a high CO<sub>2</sub> capacity (1.27 mmol·g<sup>-1</sup>) in flue gas at 75 °C. This strategy has the advantages of a simple, green, and efficient preparation process, and it provides a new idea for the controllable design of highly active CO<sub>2</sub> adsorbent.

**Author Contributions:** Investigation, methodology, visualization, writing—original draft, and formal analysis, M.Q.; methodology, H.W.; visualization, Y.H.; formal analysis, H.G., D.G. and F.P.; supervision, conceptualization, funding acquisition, and writing—review and editing, L.S. and Q.Y. All authors have read and agreed to the published version of the manuscript.

**Funding:** This research was funded by the Knowledge Innovation Program of Wuhan Basic Research (2022020801010354), the Joint Fund of the Yulin University and the Dalian National Laboratory for Clean Energy (Grant YLU-DNL Fund 2021021), the National Natural Science Foundation of China (51776133; U1810125), and the Shanxi-Zheda Institute of Advanced Materials and Chemical Engineering (2022SX-TD015).

**Institutional Review Board Statement:** Not applicable.

**Informed Consent Statement:** Not applicable.

**Data Availability Statement:** Not applicable.

**Conflicts of Interest:** The authors declare no conflict of interest.

**Sample Availability:** Samples of the compounds are not available from the authors.

#### References

1. Doney, S.C.; Busch, D.S.; Cooley, S.R.; Kroeker, K.J. The Impacts of Ocean Acidification on Marine Ecosystems and Reliant Human Communities. *Annu. Rev. Environ. Resour.* **2020**, *45*, 83–112. [[CrossRef](#)]
2. Zhang, T.; Zhang, W.; Yang, R.; Liu, Y.; Jafari, M. CO<sub>2</sub> Capture and Storage Monitoring Based on Remote Sensing Techniques: A Review. *J. Clean. Prod.* **2021**, *281*, 124409. [[CrossRef](#)]
3. Ahmed, D.S.; El-Hiti, G.A.; Yousif, E.; Hameed, A.S.; Abdalla, M. New Eco-Friendly Phosphorus Organic Polymers as Gas Storage Media. *Polymers* **2017**, *9*, 336. [[CrossRef](#)] [[PubMed](#)]
4. Hadi, A.G.; Jawad, K.; Yousif, E.; El-Hiti, G.A.; Alotaibi, M.H.; Ahmed, D.S. Synthesis of Telmisartan Organotin(IV) Complexes and their use as Carbon Dioxide Capture Media. *Molecules* **2019**, *24*, 1631. [[CrossRef](#)] [[PubMed](#)]
5. Wang, R.; Liu, S.; Li, Q.; Zhang, S.; Wang, L.; An, S. CO<sub>2</sub> Capture Performance and Mechanism of Blended Amine Solvents Regulated By N-methylcyclohexylamine. *Energy* **2021**, *215*, 119209. [[CrossRef](#)]
6. He, X. Polyvinylamine-Based Facilitated Transport Membranes for Post-Combustion CO<sub>2</sub> Capture: Challenges and Perspectives from Materials to Processes. *Engineering* **2021**, *7*, 124–131. [[CrossRef](#)]
7. Li, Z.L.; Zhou, Y.L.; Yan, W.; Luo, L.; Su, Z.Z.; Fan, M.Z.; Wang, S.R.; Zhao, W.G. Cost-Effective Monolithic Hierarchical Carbon Cryogels with Nitrogen Doping and High-Performance Mechanical Properties for CO<sub>2</sub> Capture. *ACS Appl. Mater. Inter.* **2020**, *12*, 21748–21760. [[CrossRef](#)]
8. Xu, L.; Xing, C.Y.; Ke, D.; Chen, L.; Qiu, Z.J.; Zeng, S.L.; Li, B.J.; Zhang, S. Amino-Functionalized beta-Cyclodextrin to Construct Green Metal-Organic Framework Materials for CO<sub>2</sub> Capture. *ACS Appl. Mater. Inter.* **2020**, *12*, 3032–3041. [[CrossRef](#)]
9. Faria, A.C.; Trujillano, R.; Rives, V.; Miguel, C.V.; Rodrigues, A.E.; Madeira, L.M. Alkali metal (Na, Cs and K) Promoted Hydrotalcites for High Temperature CO<sub>2</sub> Capture from Flue Gas in Cyclic Adsorption Processes. *Chem. Eng. J.* **2022**, *427*, 131502. [[CrossRef](#)]
10. Omer, R.M.; Al-Tikrity, E.T.B.; El-Hiti, G.A.; Alotibi, M.F.; Ahmed, D.S.; Yousif, E. Porous Aromatic Melamine Schiff Bases as Highly Efficient Media for Carbon Dioxide Storage. *Processes* **2019**, *8*, 17. [[CrossRef](#)]
11. Shi, X.; Xiao, H.; Azarabadi, H.; Song, J.; Wu, X.; Chen, X.; Lackner, K.S. Sorbents for the Direct Capture of CO<sub>2</sub> from Ambient Air. *Angew. Chem. Int. Ed.* **2020**, *59*, 6984–7006. [[CrossRef](#)]

12. Choi, H.J.; Min, J.G.; Ahn, S.H.; Shin, J.; Hong, S.B.; Radhakrishnan, S.; Chandran, C.V.; Bell, R.G.; Breynaert, E.; Kirschhock, C.E.A. Framework Flexibility-Driven CO<sub>2</sub> Adsorption on a Zeolite. *Mater. Horiz.* **2020**, *7*, 1528–1532. [[CrossRef](#)]
13. Rattanaphan, S.; Rungrotmongkol, T.; Kongsune, P. Biogas Improving by Adsorption of CO<sub>2</sub> on Modified Waste Tea Activated Carbon. *Renew. Energy* **2020**, *145*, 622–631. [[CrossRef](#)]
14. Chen, C.; Xu, H.; Jiang, Q.; Lin, Z. Rational Design of Silicas with Meso-Macroporosity as Supports for High-Performance Solid Amine CO<sub>2</sub> Adsorbents. *Energy* **2021**, *214*, 119093. [[CrossRef](#)]
15. Vadillo, J.M.; Gómez-Coma, L.; Garea, A.; Irabien, A. Hollow Fiber Membrane Contactors in CO<sub>2</sub> Desorption: A Review. *Energy Fuels* **2020**, *35*, 111–136. [[CrossRef](#)]
16. Lee, R.J.; Jawad, Z.A.; Ahmad, A.L.; Chua, H.B. Incorporation of Functionalized Multi-Walled Carbon Nanotubes (MWCNTs) into Cellulose Acetate Butyrate (CAB) Polymeric Matrix to Improve the CO<sub>2</sub>/N<sub>2</sub> Separation. *Process Saf. Environ.* **2018**, *117*, 159–167. [[CrossRef](#)]
17. Chen, M.; Xu, J.; You, Z.; Dong, Y.; Yuan, H.; Yin, J.; Zhou, X. Synergetic Effect of Liquid/Plasma on Wet Wheat Straw Porous Carbon: Pore Structure, Heteroatom Doping and CO<sub>2</sub> adsorption. *Mater. Lett.* **2020**, *262*, 127185. [[CrossRef](#)]
18. Mutyala, S.; Jonnalagadda, M.; Ibrahim, S.M. Effect of Modification of UiO-66 for CO<sub>2</sub> Adsorption and Separation of CO<sub>2</sub>/CH<sub>4</sub>. *J. Mol. Struct.* **2021**, *1227*, 129506. [[CrossRef](#)]
19. Gautam, S.; Cole, D. CO<sub>2</sub> Adsorption in Metal-Organic Framework Mg-MOF-74: Effects of Inter-Crystalline Space. *Nanomaterials* **2020**, *10*, 2274. [[CrossRef](#)]
20. Wang, J.; Wang, F.; Duan, H.; Li, Y.; Xu, J.; Huang, Y.; Liu, B.; Zhang, T. Polyvinyl Chloride-Derived Carbon Spheres for CO<sub>2</sub> Adsorption. *ChemSusChem* **2020**, *13*, 6426–6432.
21. Avci, G.; Erucar, I.; Keskin, S. Do New MOFs Perform Better for CO<sub>2</sub> Capture and H<sub>2</sub> Purification? Computational Screening of the Updated MOF Database. *ACS. Appl. Mater. Inter.* **2020**, *12*, 41567–41579. [[CrossRef](#)] [[PubMed](#)]
22. Hisaki, I.; Xin, C.; Takahashi, K.; Nakamura, T. Designing Hydrogen-Bonded Organic Frameworks (HOFs) with Permanent Porosity. *Angew. Chem. Int. Ed.* **2019**, *58*, 11160–11170. [[CrossRef](#)] [[PubMed](#)]
23. Zeng, Y.; Zou, R.; Zhao, Y. Covalent Organic Frameworks for CO<sub>2</sub> Capture. *Adv. Mater.* **2016**, *28*, 2855–2873. [[CrossRef](#)] [[PubMed](#)]
24. Inukai, M.; Tamura, M.; Horike, S.; Higuchi, M.; Kitagawa, S.; Nakamura, K. Storage of CO<sub>2</sub> into Porous Coordination Polymer Controlled by Molecular Rotor Dynamics. *Angew. Chem. Int. Ed.* **2018**, *57*, 8687–8690. [[CrossRef](#)]
25. Lin, Y.; Chen, Y.; Yu, Z.; Huang, Z.; Lai, J.-C.; Tok, J.B.H.; Cui, Y.; Bao, Z. Reprocessable and Recyclable Polymer Network Electrolytes via Incorporation of Dynamic Covalent Bonds. *Chem. Mater.* **2022**, *34*, 2393–2399. [[CrossRef](#)]
26. Afrose, S.P.; Mahato, C.; Sharma, P.; Roy, L.; Das, D. Nonequilibrium Catalytic Supramolecular Assemblies of Melamine- and Imidazole-Based Dynamic Building Blocks. *J. Am. Chem. Soc.* **2022**, *144*, 673–678. [[CrossRef](#)]
27. Blanke, M.; Postulka, L.; Ciara, I.; D’Acierno, F.; Hildebrandt, M.; Gutmann, J.S.; Dong, R.Y.; Michal, C.A.; Giese, M. Manipulation of Liquid Crystalline Properties by Dynamic Covalent Chemistry horizontal line En Route to Adaptive Materials. *ACS. Appl. Mater. Inter.* **2022**, *14*, 16755–16763. [[CrossRef](#)]
28. Chen, S.; Liu, M.; Zhang, J.; Zhang, Z.; Zhu, J.; Pan, X.; Zhu, X. Photoresponsive Dynamic Covalent Bond Based On Addition–Fragmentation Chain Transfer of Allyl Selenides. *Polym. Chem.* **2021**, *12*, 1622–1626. [[CrossRef](#)]
29. Vo, T.K.; Kim, W.-S.; Kim, J. Ethylenediamine-incorporated MIL-101(Cr)-NH<sub>2</sub> Metal-Organic Frameworks for Enhanced CO<sub>2</sub> Adsorption. *Korean J. Chem. Eng.* **2020**, *37*, 1206–1211. [[CrossRef](#)]
30. Sanz-Pérez, E.S.; Lobato, B.; Lopez-Anton, M.A.; Arencibia, A.; Sanz, R.; Martínez-Tarazona, M.R. Effectiveness of Amino-Functionalized Sorbents for CO<sub>2</sub> Capture in the Presence of Hg. *Fuel* **2020**, *267*, 117250. [[CrossRef](#)]
31. Guo, Y.; Luo, L.; Zheng, Y.; Zhu, T. Optimization of CO<sub>2</sub> Adsorption on Solid-Supported Amines and Thermal Regeneration Mode Comparison. *ACS Omega* **2020**, *5*, 9641–9648. [[CrossRef](#)] [[PubMed](#)]
32. Wang, D.; Xue, Y.; Wang, C.; Ji, J.; Zhou, Z.; Tang, C. Improved Capture of Carbon Dioxide and Methane via Adding Micropores Within Porous Boron Nitride Fibers. *J. Mater. Sci.* **2019**, *54*, 10168–10178. [[CrossRef](#)]
33. Rehman, A.; Farrukh, S.; Hussain, A.; Fan, X.; Pervaiz, E. Adsorption of CO<sub>2</sub> on amine-functionalized green metal-organic framework: An interaction between amine and CO<sub>2</sub> molecules. *Environ. Sci. Pollut. Res. Int.* **2019**, *26*, 36214–36225. [[CrossRef](#)] [[PubMed](#)]
34. Putz, A.M.; Ciopec, M.; Negrea, A.; Grad, O.; Ianasi, C.; Ivankov, O.I.; Milanovic, M.; Stijepovic, I.; Almas, L. Comparison of Structure and Adsorption Properties of Mesoporous Silica Functionalized with Aminopropyl Groups by the Co-Condensation and the Post Grafting Methods. *Materials* **2021**, *14*, 628. [[CrossRef](#)]
35. Lawson, S.; Griffin, C.; Rapp, K.; Rownaghi, A.A.; Rezaei, F. Amine-Functionalized MIL-101 Monoliths for CO<sub>2</sub> Removal from Enclosed Environments. *Energy Fuels* **2019**, *33*, 2399–2407. [[CrossRef](#)]
36. De ON Ribeiro, J.; Nunes, E.H.M.; Vasconcelos, D.C.L.; Vasconcelos, W.L.; Nascimento, J.F.; Grava, W.M.; Derks, P.W.J. Role of the Type of Grafting Solvent and Its Removal Process on APTES Functionalization onto SBA-15 Silica for CO<sub>2</sub> Adsorption. *J. Porous Mater.* **2019**, *26*, 1581–1591. [[CrossRef](#)]
37. Ji, C.; Huang, X.; Li, L.; Xiao, F.; Zhao, N.; Wei, W. Pentaethylenhexamine-Loaded Hierarchically Porous Silica for CO<sub>2</sub> Adsorption. *Materials* **2016**, *9*, 835. [[CrossRef](#)]
38. Xie, W.; Huang, S.; Tang, D.; Liu, S.; Zhao, J. Biomass-derived Schiff Base Compound Enabled Fire-Safe Epoxy Thermoset with Excellent Mechanical Properties and High Glass Transition Temperature. *Chem. Eng. J.* **2020**, *394*, 123667. [[CrossRef](#)]

39. Liu, X.; Liang, L.; Lu, M.; Song, X.; Liu, H.; Chen, G. Water-Resistant Bio-Based Vitrimers Based on Dynamic Imine Bonds: Self-healability, Remodelability and Ecofriendly Recyclability. *Polymer* **2020**, *210*, 123030. [[CrossRef](#)]
40. Wang, Y.; Xiao, G.; Peng, Y.; Chen, L.; Fu, S. Effects of Cellulose Nanofibrils on Dialdehyde Carboxymethyl Cellulose Based Dual Responsive Self-Healing Hydrogel. *Cellulose* **2019**, *26*, 8813–8827. [[CrossRef](#)]
41. He, X.; Yang, Y.; Wu, H.; He, G.; Xu, Z.; Kong, Y.; Cao, L.; Shi, B.; Zhang, Z.; Tongsh, C.; et al. De Novo Design of Covalent Organic Framework Membranes toward Ultrafast Anion Transport. *Adv. Mater.* **2020**, *32*, e2001284. [[CrossRef](#)] [[PubMed](#)]
42. Fan, C.; Wu, H.; Guan, J.; You, X.; Yang, C.; Wang, X.; Cao, L.; Shi, B.; Peng, Q.; Kong, Y.; et al. Scalable Fabrication of Crystalline COF Membranes from Amorphous Polymeric Membranes. *Angew. Chem. Int. Ed.* **2021**, *60*, 18051–18058. [[CrossRef](#)] [[PubMed](#)]
43. Wehner, M.; Würthner, F. Supramolecular polymerization through kinetic pathway control and living chain growth. *Nat. Rev. Chem.* **2019**, *4*, 38–53. [[CrossRef](#)]
44. Adelizzi, B.; Aloï, A.; Markvoort, A.J.; Ten Eikelder, H.M.M.; Voets, I.K.; Palmans, A.R.A.; Meijer, E.W. Supramolecular block copolymers under thermodynamic control. *J. Am. Chem. Soc.* **2018**, *140*, 7168–7175. [[CrossRef](#)] [[PubMed](#)]
45. Vantomme, G.; Ter Huurne, G.M.; Kulkarni, C.; Ten Eikelder, H.M.M.; Markvoort, A.J.; Palmans, A.R.A.; Meijer, E.W. Tuning the length of cooperative supramolecular polymers under thermodynamic control. *J. Am. Chem. Soc.* **2019**, *141*, 18278–18285. [[CrossRef](#)] [[PubMed](#)]
46. Zhao, S.; Jiang, C.; Fan, J.; Hong, S.; Mei, P.; Yao, R.; Liu, Y.; Zhang, S.; Li, H.; Zhang, H.; et al. Hydrophilicity gradient in covalent organic frameworks for membrane distillation. *Nat. Mater.* **2021**, *20*, 1551–1558. [[CrossRef](#)]
47. Belowich, M.E.; Stoddart, J.F. Dynamic imine chemistry. *Chem. Soc. Rev.* **2012**, *41*, 2003–2024. [[CrossRef](#)]
48. Alves, L.D.S.; Moreira, B.R.A.; Viana, R.D.S.; Dias, E.S.; Rinker, D.L.; Pardo-Gimenez, A.; Zied, D.C. Spent Mushroom Substrate Is Capable of Physisorption-Chemisorption of CO<sub>2</sub>. *Environ. Res.* **2022**, *204*, 111945. [[CrossRef](#)]
49. Vitaku, E.; Dichtel, W.R. Synthesis of 2D Imine-Linked Covalent Organic Frameworks through Formal Transimination Reactions. *J. Am. Chem. Soc.* **2017**, *139*, 12911–12914. [[CrossRef](#)]
50. Shan, Z.; Wu, X.; Xu, B.; Hong, Y.L.; Wu, M.; Wang, Y.; Nishiyama, Y.; Zhu, J.; Horike, S.; Kitagawa, S.; et al. Dynamic Transformation between Covalent Organic Frameworks and Discrete Organic Cages. *J. Am. Chem. Soc.* **2020**, *142*, 21279–21284. [[CrossRef](#)]
51. Mao, H.Y.; Tang, J.; Day, G.S.; Peng, Y.C.; Wang, H.Z.; Xiao, X.; Yang, Y.F.; Jiang, Y.W.; Chen, S.; Halat, D.M.; et al. A scalable solid-state nanoporous network with atomic-level interaction design for carbon dioxide capture. *Sci. Adv.* **2022**, *8*, eabo6849. [[CrossRef](#)] [[PubMed](#)]
52. Ma, X.; Yang, Y.; Wu, Q.; Liu, B.; Li, D.; Chen, R.; Wang, C.; Li, H.; Zeng, Z.; Li, L. Underlying Mechanism of CO<sub>2</sub> Uptake onto Biomass-Based Porous Carbons: Do Adsorbents Capture CO<sub>2</sub> Chiefly Through Narrow Micropores? *Fuel* **2020**, *282*, 118727. [[CrossRef](#)]
53. Kong, W.; Liu, J. Ordered Mesoporous Carbon with Enhanced Porosity to Support Organic Amines: Efficient Nanocomposites for the Selective Capture of CO<sub>2</sub>. *New J. Chem.* **2019**, *43*, 6040–6047. [[CrossRef](#)]
54. Alkadhem, A.M.; Elgzoly, M.A.A.; Onaizi, S.A. Novel Amine-Functionalized Magnesium Oxide Adsorbents for CO<sub>2</sub> Capture at Ambient Conditions. *J. Environ. Chem. Eng.* **2020**, *8*, 103968. [[CrossRef](#)]
55. Fang, Q.; Huang, W.; Wang, H. Role of Additives in Silica-Supported Polyethylenimine Adsorbents for CO<sub>2</sub> Adsorption. *Mater. Res. Express* **2020**, *7*, 035026. [[CrossRef](#)]
56. Mohamad, N.A.; Zubair, N.A.; Lotf, E.A.; Nasef, M.M.; Ahmad, A.; Ali, R.R.; Abdullah, T.A.T.; Ting, T.M. Effect of Ligand Type on CO<sub>2</sub> Adsorption over Amine Functionalized Fibrous Adsorbents. *IOP Conf. Ser. Mater. Sci. Eng.* **2020**, *808*, 012009. [[CrossRef](#)]
57. Rong, X.; Ettelaie, R.; Lishchuk, S.V.; Cheng, H.; Zhao, N.; Xiao, F.; Cheng, F.; Yang, H. Liquid Marble-Derived Solid-Liquid Hybrid Superparticles for CO<sub>2</sub> Capture. *Nat. Commun.* **2019**, *10*, 1854. [[CrossRef](#)]